

# Computational and experimental visualization in heat and mass transfer problems

T.A. Kowalewski<sup>1\*</sup> W.J. Hiller<sup>2</sup> & G. de Vahl Davis<sup>3</sup>

<sup>1</sup>Institute of Fundamental Technological Research, PL-00-049 Warszawa

<sup>2</sup>Max-Planck-Institut für Strömungsforschung, D-37073 Göttingen

<sup>3</sup>University of New South Wales, Kensington, 2033 Australia

## ABSTRACT

Validation and improvement of theoretical models and numerical results using experimental data is one of the most challenging research goals nowadays. With this objective a new experimental technique was developed and applied to the study of heat and mass transfer problems in fluid flows. The method, based on a computational analysis of the colour and displacement of liquid crystal tracers, was used to determine both the temperature and velocity fields of natural convection flow within a rectangular enclosure. The paths of the individual tracers were obtained using 3-D particle tracking. Comparison of several experimental and numerical results will be discussed.

## 1. INTRODUCTION

With the growing capacity of computers and the continuing improvement of numerical codes, the question of the exactness of numerical solutions to describe real fluid flow is of primary importance. Results obtained from idealised models often offer information only about the global description of flow behaviour. There is however a wide class of practical problems where knowledge of just the general behaviour of flow is not sufficient to obtain a full quantitative description of the phenomena. Examples include the distribution of fuel or soot in a combustion chamber, the transport of impurities in crystal growth, and the propagation of pollution in air and water. In such cases the knowledge of some specific flow details is necessary for the full control of the investigated phenomenon.

Particle trajectories are a good example of where discrepancies between observed and simulated results can occur. Due to the strong sensitivity of particle position to small additional forces or numerical inaccuracy, it can often be detected that observed and simulated trajectories are far from being in acceptable agreement, even for well known *standard* problems. One of the reasons is the three

dimensional character of the flow complicating its numerical modeling. Also thermal boundary conditions taken at non-isothermal walls are in practice neither perfectly adiabatic, nor perfectly heat conducting, as is usually assumed in numerical models. In addition, the widely used Boussinesq approximation for the physical determination of the fluid flow is not strictly valid for real fluids. In particular, dependence of viscosity on temperature for such liquids as glycerin or oils may generate severe discrepancies between expected and observed flow pattern.

The aim of the paper is to review our attempts to understand and explain observed discrepancies between measured and calculated convective flow patterns. It is a summary of the work which the authors have been fortunate to share with their colleagues and students at the Max-Planck-Institut and at the University of New South Wales. In particular we would like to acknowledge the contribution of St. Koch, C. Abegg, P. Mitgau and C. Soeller from MPL. Thanks to them the experimental investigations could be realised. Our thanks are also due to E. Leonardi and G. Yeoh (University of New South Wales) and F. Stella (University of Rome) for their valuable support in the numerical modeling of the flow, including access to their computer codes.

A new visualization technique, based on the application of unencapsulated liquid crystals as tracers [1], has been developed to study convective flow (see Fig.1). Computerised analysis of the colour and displacement of the liquid crystal tracers has the great advantage of enabling the acquisition of both the temperature and velocity fields [2, 3]. The paths of the individual tracers have been followed using 3-D particle tracking [4]. These experimental observations have been compared with the corresponding numerical results. Numerical simulations of transient and steady states have been performed using velocity-vector potential (FRECON3D [5], FREEZE3D [6]) and velocity-vorticity (TRFLOW [7]) finite difference formulations of 3-D Navier-Stokes. The computational models have been adopted to simulate as closely as possible the physical experiment. Specifically, either the heat flux through the non-isothermal

---

\*Temporary at Max-Planck-Institut für Strömungsforschung.

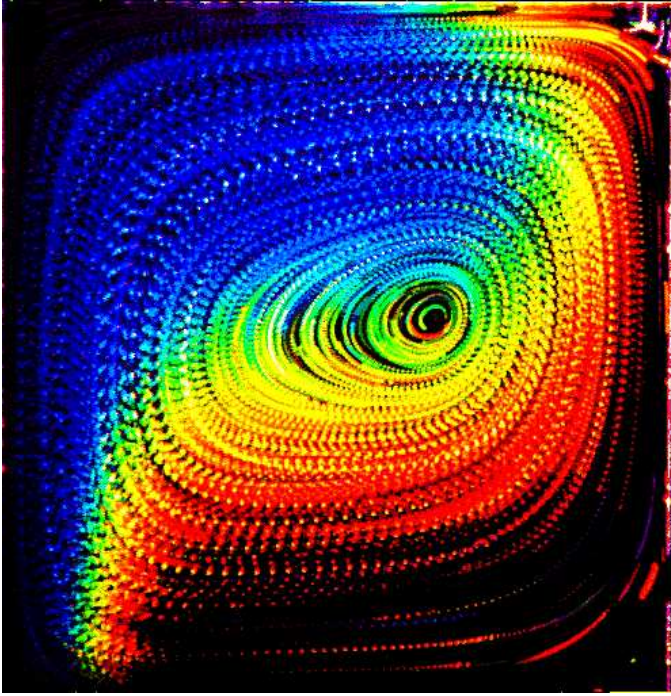


Figure 1: Multiexposure colour photograph of the convective flow with liquid crystal tracers. The vertical centre plane  $z=0.5$ ,  $Pr = 6900$ ,  $Ra = 1.1 \cdot 10^4$ .

walls has been computed to match the measured wall temperature, or the measured values of the temperature of the walls were used in the calculations. Also the effect of variable fluid properties on the resulting simulation was checked.

In our experimental and numerical studies we mainly concentrated our attention on the idealised “bench mark” case of steady and transient flow in a cubical cavity with differentially heated end walls. It is one of the most popular test problems to verify numerical solutions of the Navier-Stokes equations [8]. In addition to its theoretical interest, this type of convective flow has numerous possible practical applications, among which probably the most popular one is that of double glazing. Other applications can be found in nuclear reactors, energy storage containers, ventilation of rooms and crystal growth in liquids.

## 2. PROBLEM DESCRIPTION

We consider the convective flow in a cubical box filled with a viscous heat conducting liquid. The fluid density is temperature dependent. In some studies viscosity, thermal conductivity and heat capacity are also assumed to be temperature dependent. Two cases of convection were investigated, which we designate the differentially heated cavity and the lid-cooled cavity. In the first configuration, see Fig. 2a, two opposite, vertical walls of the cube are isothermal at temperatures  $T_h$  (hot) and  $T_c$  (cold), respectively. The other four walls are nominally insulators of finite thermal diffusivity. Due to temperature gradients existing between the fluid inside the cavity and the surrounding atmosphere and also along the front and back walls, the lid and the floor of the box, a heat flux both through and

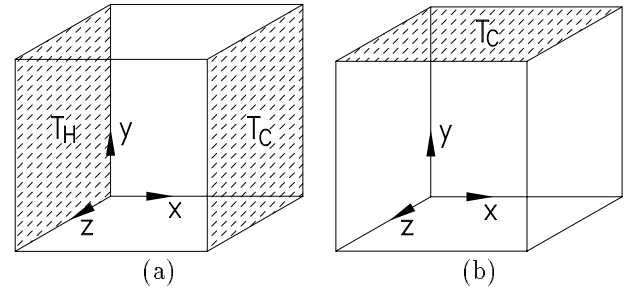


Figure 2: The cubical box. The  $y$ -axis is parallel to the gravity vector  $\vec{g}$ . (a) Differentially heated cavity; (b) lid-cooled cavity.

along the walls is generated.

In the second configuration, the top wall of the cube is isothermal at the temperature  $T_c$ , whereas the other five walls are non-adiabatic, allowing a heat flux from the external fluid surrounding the box, Fig. 2b. The temperature of the external bath  $T_h > T_c$  is kept constant. Due to forced convection in the bath it can be assumed that the temperature at the external surfaces of the box is constant and equals  $T_h$ . The temperature field at the inner surfaces of the walls adjusts itself depending on both the flow inside the box and the heat flux through and along the walls. This configuration has been selected to investigate convective flow with a phase change (freezing of water at the top wall).

Two dimensionless characteristic parameters defining the problem, the Rayleigh number

$$Ra = \frac{g\beta\Delta T l^3}{\kappa\nu} \quad (1)$$

and the Prandtl number

$$Pr = \frac{\nu}{\kappa}, \quad (2)$$

are chosen to compare the numerical and experimental results.

In the above definitions,  $g$ ,  $l$ ,  $\Delta T$ ,  $\kappa$ ,  $\beta$ ,  $\nu$  denote respectively the gravitational acceleration, the cavity dimension, the temperatures difference  $T_h - T_c$ , the thermal diffusivity, the coefficient of thermal expansion and the kinematic viscosity. The non-dimensional temperature is defined as:  $\theta = (T - T_c)/\Delta T$ .

The flow structure in the differentially heated cavity strongly depends on the Rayleigh number. At a small Rayleigh number ( $Ra < 10^3$ ) the flow is dominated by conduction, which is seen in the form of vertical isotherms across the cavity. Convection is negligible in comparison with horizontal heat conduction in the medium, and the corresponding isotherms are parallel to the heated walls. In the parameter range analysed here ( $Ra = 2 \cdot 10^4 - 10^5$ ), both convection and conduction are significant. At the lower end of the range ( $Ra = 2 \cdot 10^4$ ), heat transfer due to convection begins to play a significant role, generating a vertical temperature gradient in the centre of the cavity. The horizontal temperature gradient is positive everywhere, giving rise to a positive vorticity generation. The streamlines correspond to a single roll, with its centre located at the centre of the cavity (Fig.3a). At higher Rayleigh numbers ( $Ra > 6 \cdot 10^4$ )

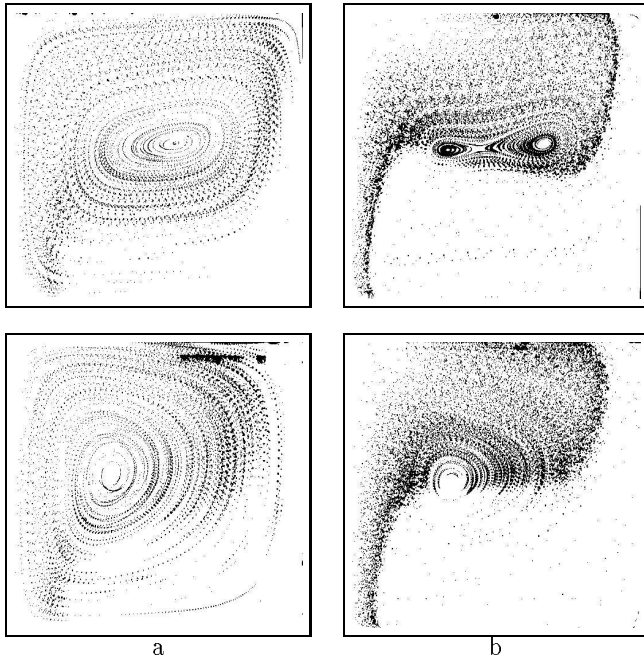


Figure 3: Multiexposure photographs of the convective flow at the vertical centre plane  $z=0.5$  (above) and the front wall  $z=0.95$  (below); glycerin ( $Pr=6300$ ) with LC tracers. (a)  $Ra = 2 \cdot 10^4$ , (b)  $Ra = 8 \cdot 10^4$

the horizontal temperature gradient becomes locally negative in some regions, promoting the generation of negative vorticity in the core. This causes horizontal elongation of the streamlines and the development of a second roll in the core (Fig.3b).

Natural convection in the cavity with a cooled top wall exhibits a more complex character. Physically this configuration has some similarity to the Rayleigh-Bénard problem. However due to the different thermal boundary conditions at the side walls the flow structure is quite different. The cubic symmetry of the box imposes a strong downward flow along the vertical axis of symmetry. Eight symmetrical flow cells are created, transporting the heated liquid upwards to the cold top wall.

### 3. EXPERIMENTAL

The experimental set-up (Fig. 4) used to acquire temperature and velocity fields consists of the convection box, a xenon flash tube and a CCD colour camera. They are mounted on a rectangular frame, which can be tilted to observe vertical and horizontal cross-sections without re-adjusting the optics. The box, of 38mm inner dimension, consists of two vertical isothermal plates, opposite to each other, made of a black anodized metal, and four 8 mm thick plexiglas walls. The isothermal walls are maintained at a constant temperature by a water flowing through internal channels in the plates. The temperature of the water is controlled by thermostats. As a flow medium, pure glycerin, its aqueous solutions and pure water were used. Depending on the liquid composition and by varying the temperature difference  $\Delta T$  it was possible to cover a relatively wide range

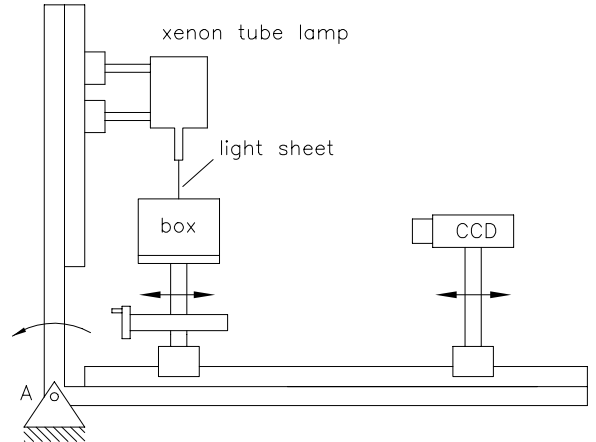


Figure 4: Experimental set-up used to measure temperature and velocity fields in the convection cavity.

of Rayleigh and Prandtl numbers: ( $Ra = 2 \cdot 10^4 - 3 \cdot 10^6$ ,  $Pr = 7 - 6900$ ). The temperature and velocity fields were measured by means of liquid crystals (LC) suspended as small tracer particles in the liquid. The visualization of temperature using thermochromic liquid crystals is based on their temperature-dependent reflectivity at the visible light wavelengths. If the liquid crystals are illuminated with white light, then the colour of the light they reflect changes from red to blue when the temperature is raised. This occurs within a well defined temperature range (the so called colour play range), which depends on the type of LC used. The LCs which we used here are TM107 (temperature range  $27^\circ - 32^\circ C$ ) and TM317 ( $20^\circ - 23^\circ C$ ) manufactured by BDH Chemicals Ltd.

The flow is observed at the vertical and horizontal cross sections of the cavity using a light sheet technique. The xenon flash tube generates a 2 mm thick sheet of white light, which illuminates the selected cross-section of the flow. A three chip CCD colour camera (Sony DXC-750P), which gives an RGB-signal for the red, green and blue components of the incoming light, is used to observe the flow. The images are acquired by three identical 8-bit frame grabbers (PPI- Eltec) in a VME-bus computer. It was also found valuable to acquire subsequent red, green and blue portions of the video signal employing only one frame grabber (VFG Imaging Inc.).

The recording of the flow patterns and temperature fields is performed periodically. Investigating transient flow patterns, every 30-60s the recorded digitized images are stored on the hard disk of the computer for later evaluation. Three-dimensional flow structures have been recorded for the steady state only. Moving the convection cavity relative to the illuminating light sheet the entire flow field can be scanned successively. Besides the further image processing, the computer also controlled the experimental conditions, i.e. the wall temperatures, position of the cavity and recording sequences.

#### 3.1. Temperature measurements

As previously mentioned, the cavity is filled with a very dilute suspension of uncoated thermochromic liquid crystal droplets in a glycerin-water mixture. The mean diameter of the LC particles is about  $50\mu m$ . The particles are used

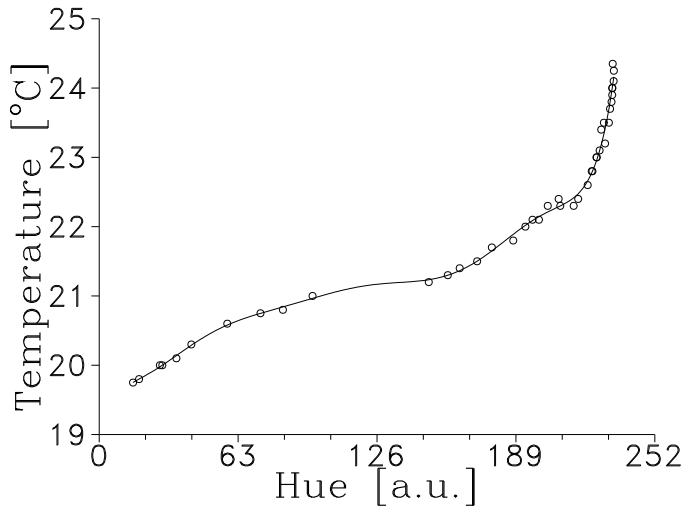


Figure 5: Typical calibration curve. The hue values of RGB colours are (0,126,252), respectively.

both as tracers for the velocity evaluation and as local temperature sensors. For evaluating the temperature, what is known as the *HSI* representation [3] of the *RGB* space is used. The incoming *RGB* signals are transformed pixel by pixel into intensity, saturation and hue. Temperature is determined by relating the hue to a temperature calibration function. The non-linear relation between temperature and hue (predetermined by the camera construction) is described by a 9th order polynomial fitted to the measured points (Fig.5). The accuracy of the measured temperature depends on the hue value, and varies in the temperature range 20 – 24°C from  $\pm 0.1K$  to  $\pm 0.3K$ .

### 3.2. Velocity measurements

The 2-D velocity vector distribution has been measured by particle image velocimetry (PIV). By this method the motion of the scattering particles observed in the plane of the illuminating light sheet can be analysed. Usually PIV techniques apply an autocorrelation method for double-exposed photographic images. It offers high temporal resolution, but the analysis gives only the length and angle of the displacement vector, and not its sign. The method applied here [9] uses two separately captured digital images taken at a constant time interval (typically 5s) to evaluate the motion of the particles. Each of the images taken shows a relatively dense cloud of single illuminated particles (LCs). The magnitude and direction of the velocity vectors are determined using a correlation analysis. This is done by dividing the whole image (typically 512x512 pixels) into 64x64 pixel matrices, which are spaced every 32 pixels (partly overlapping each other). The correlation of the corresponding matrices of both images allows the evaluation of the mean translation vector for each group of particles simultaneously detected in both matrices. The evaluation of images has been performed on an IBM RS6000-350 workstation.

### 3.3. Particle Tracks

To obtain a general view of the flow pattern several images recorded periodically within a given time interval have been added in the computer memory. Displayed images

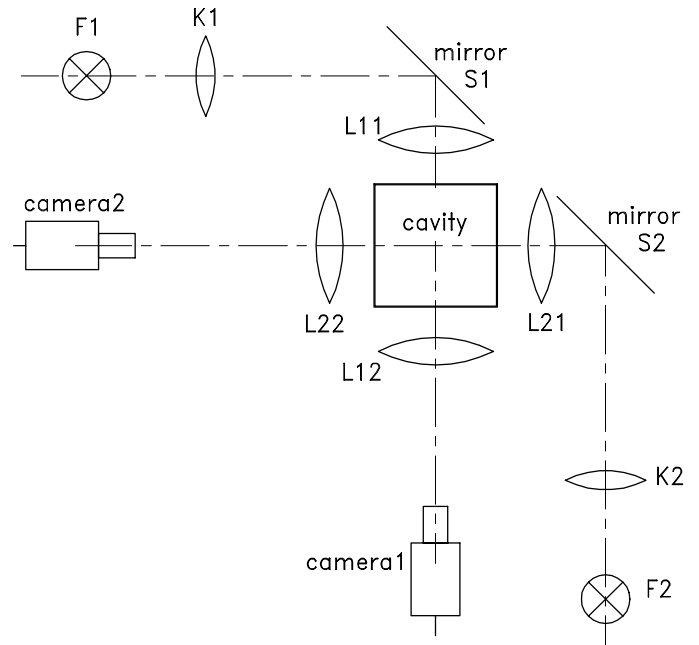


Figure 6: Experimental set-up for 3-D particle tracking. Two isothermal walls of the cavity are parallel to the plane of the figure.

are similar to the multiexposed photographs, showing the flow direction and its structure. However, only the two-dimensional projection of the particle tracks can be acquired this way. As the flow is usually strongly three-dimensional, a comparison with the calculated particle tracks is possible only using stereoscopic observations.

For this purpose a special procedure has been developed [4], which allows the detection and full automatic tracking of particles suspended in the flow medium. The images were captured by two CCD cameras (Sony XC77CE) integrated with two identical frame grabbers (VFG Imaging Inc.) installed in a personal computer. A few, nearly neutrally buoyant tracers of a diameter of about  $150\mu$  were observed against a bright background from two perpendicular directions (Fig. 6). The evaluation software allows the identification of particles and the storage of data over periods as long as several days. Several runs have been performed using relatively large particles ( $400\mu$  in diameter) to find effects of the finite mass, size and density difference of the tracers on the acquired tracks. Both positive and negative particle-liquid density differences have been studied [10].

## 4. NUMERICAL MODELS

In conjunction with the experimental program, a numerical simulation of the problem has been performed using a finite difference model of the Navier-Stokes and energy equations. By taking the curl of N-S equation in terms of primitive variables, one obtains the vorticity transport equation for an incompressible fluid, which is the basic equation of

motion for all codes used here:

$$\frac{1}{Pr} \frac{\partial \vec{\omega}}{\partial t} + \frac{1}{Pr} \nabla \times (\vec{\omega} \times \vec{u}) = \nabla^2 \vec{\omega} - Ra \nabla \times \left( \theta \frac{\vec{g}}{|g|} \right) \quad (3)$$

The velocity field must also satisfy the equation of continuity:

$$\nabla \cdot \vec{u} = 0 \quad (4)$$

The energy equation is given in its standard form:

$$\frac{\partial \theta}{\partial t} + (\vec{u} \cdot \nabla) \theta = \nabla^2 \theta . \quad (5)$$

As we have already mentioned, three numerical codes have been used in our investigations: FRECON3D [5] which is a superior false transient solver for all studies of steady convection of a constant property fluid; TRFLOW [7] which is a relatively flexible code allowing both two- and three dimensional simulation of transient convection; and the most complex code FREEZE3D [6], developed generally to study convection with phase changes in a fluid with temperature-dependent properties. Below we summarize the main features of these models.

#### 4.1. FRECON3D

The equations governing the flow of a constant property incompressible fluid are the vorticity transport equations (3). The Boussinesq approximation is used: the density is assumed constant except for the buoyancy term of the equation of motion. The thermal conductivity, viscosity and specific heat of the fluid are assumed to be constant. The vorticity and the vector potential formulation [11] is used. The continuity equation shows that the velocity vector field is solenoidal. The div curl of any vector field is identically zero. It is possible then to represent the solenoidal velocity vector field by another vector field such as

$$\vec{u} = \nabla \times \vec{\Psi} \quad (6)$$

The variable  $\vec{\Psi}$  is known as the vector potential. Introducing the vorticity vector  $\vec{\omega}$

$$\vec{\omega} = \nabla \times \vec{u} \quad (7)$$

and substituting for  $\vec{u}$  in terms of  $\vec{\Psi}$  using (6), we obtain a simple relationship between the vorticity and vector potential:

$$\vec{\omega} = -\nabla^2 \vec{\Psi} \quad (8)$$

Using the definition of velocity (6) in the vorticity transport equation (3) one obtains the final form of the N-S equation in terms of  $(\vec{\omega}, \vec{\Psi})$ . The pressure is eliminated as a solution variable and the continuity equation is automatically satisfied. To speed up convergence the false transient method [12] is used. Hence, the governing equations are parabolised in time allowing their exact solution for the steady state only.

#### 4.2. TRFLOW

The Boussinesq approximation has been used in the numerical model and the equations are written in the vorticity-velocity form [7].

The equations for the velocities are obtained by taking the appropriate derivatives of vorticity (7) and using the

continuity equation (4). This yields the Poisson type equation:

$$\nabla^2 \vec{u} = -\nabla \times \vec{\omega} . \quad (9)$$

The complete set of equations used in the numerical simulation consists of eq. (3), (5) and (9).

The selection of the vorticity-velocity formulation allows the use of kinematic boundary conditions for the chosen variables in a very simple way. A time-dependent algorithm with inner iterations on all governing equations for each time step has been used to solve the case of transient heating of the cavity.

#### 4.3. FREEZE3D

The three-dimensional, variable property code FREEZE3D has been recently developed by Yeoh [6] to study phase change (solidification) problems in rectangular cavities. Here it has been employed to model the solidification experiment with water in the lid cooled cavity. Because FREEZE3D allows for the use of temperature-dependent thermodynamic and transport properties of the fluid it was also used to verify the effects of variable properties of the liquid (glycerin) in a single phase convective flow. When variable properties are investigated, the non-dimensional description of the problem is possible only formally. This is because the fluid properties, temperature, etc. have to be implemented as dimensional boundary conditions to specify the problem appropriately. For ease of comparison with many experimental and numerical results, the non-dimensional parameters are retained. Their values are calculated at a reference temperature, which in our case was the cold wall temperature  $T_c$ . The constant-property simulations have been performed with the physical fluid parameters calculated at the mean temperature  $(T_h + T_c)/2$ . In the case of strongly temperature dependent liquids (like glycerin) it may lead to an almost 50% difference in the formal values of Rayleigh and Prandtl numbers.

The governing equations of motion are based on an  $(\vec{\omega}, \vec{\Psi})$  representation of the transient vorticity transport equation (3). If convection and phase change take place, the movement of the solid-liquid interface is computed with the use of an energy balance at the interface which incorporates the latent energy transfer which accompanies phase change. As the physical domain changes, the interface boundary must be generated at each time step, following which a new computational grid is determined in the liquid and solid regions. Independent conservation equations are solved for each phase and are coupled by the condition at the solid-liquid interface. Transformation techniques have been used to map the moving physical domain onto the computational domain.

#### 4.4. Thermal boundary conditions

When simulating experimental conditions, the main problem which arises is a proper definition of thermal boundary conditions. In each code, the thermal boundary conditions are sufficiently flexible to allow the imposition of an arbitrary temperature, a specified heat flux or a specified heat transfer coefficient on each of the six surfaces of the box. In the present study, either two opposite vertical walls or the horizontal top wall are assumed to be isothermal. The boundary conditions on the remaining walls, which are not strictly either adiabatic or isothermal, were approximated by assuming a constant heat flux through each wall. This heat flux was estimated by using heat transfer

theory applied to a thick, infinitely wide plane plate of uniform conductivity into an external unlimited environment. The non-dimensional condition for the temperature  $\theta$  at the boundary can be written in the general form as

$$a\theta + b\frac{\partial\theta}{\partial n} = c \quad (10)$$

The constants  $a$ ,  $b$  and  $c$  can be varied to specify the boundary condition existing in the simulated experiment.

#### 4.5. Visualization of numerical results

To check the validity of the numerical solution in comparison with the experimental results, several methods of numerical visualization were applied. In the first step the general flow characteristics, like two-dimensional temperature and velocity fields were extracted from the calculated binary files and displayed using the graphic tool Tecplot (Amtec Eng. Inc).

A detailed visualization of the calculated flow structures can be achieved with the help of particle tracks obtained through the integration of the velocity equations. To come closer to the physical experiment the effects of additional forces acting on the real tracer particles have been studied. In the present experimental conditions the presence of particle buoyancy, the Saffman force, and wall interaction seem to be not negligible, if long runs (of several hours) are acquired. For the representation and interpretation of the calculated and measured tracks, a 3-D display program Relation (Brosa GmbH) has been successfully employed.

The validity of the tracks has been verified in a number of ways including reduction of the time step and a reversal of all velocities to enable the track to be traversed in reverse [13]. Initially all solutions were computed on a 31 by 31 by 31 mesh, chosen as a compromise between accuracy and cost. It has been found that this mesh is more than adequate if a global description of the flow is of interest. However, the localization of singularities and the determination of fine, three-dimensional characteristics of the tracks such as the pitch of spirals appeared to be more sensitive to the mesh size, especially at higher values of the Rayleigh number. With increasing mesh sizes, several test runs of the constant property code were done to check how far the mesh size influences the form of the calculated tracks. It was found that for the investigated range of parameters a 61x61x61 mesh should be employed.

## 5. RESULTS

### 5.1. Differentially heated cavity

Initially our interest was directed towards understanding the flow in the vertical centre plane of the cavity. For this purpose the observations of flow patterns and temperature fields were performed for several systems with increasing Rayleigh numbers (from  $10^4$  to  $10^5$ ) [14]. It was found that the single roll apparent in the two dimensional visualization (Fig.3a), is actually a spiralling structure transporting liquid from the front and back walls into the centre and back. It can be well detected at relatively low Rayleigh number ( $Ra < 4 \cdot 10^4$ ). Numerical simulation (Fig.7a) exhibits a similar structure.

By increasing the Rayleigh number we observe first a horizontal elongation of the streamlines and then the formation of a secondary vortex with its centre shifted towards

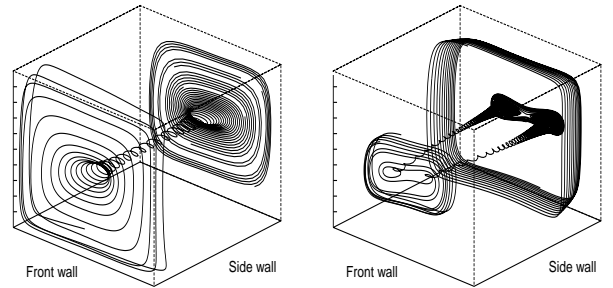


Figure 7: Calculated 3-D streamlines (front half of the cavity displayed only).  $Pr = 6300$ ; left:  $Ra = 2 \cdot 10^4$ , inner spiral runs towards centre; right:  $Ra = 7.910^4$ , two inner spirals run towards the front wall.

the warmer wall (Fig.7b). The temperature field changes very little. Fig.8 shows the measured and computed velocity and temperature fields for the two-vortex configuration ( $Ra = 1.66 \cdot 10^5$ ,  $Pr = 1109$ ).

However, in the numerical simulation adiabatic thermal boundary conditions (TBCs) have been assumed for the side walls, comparison of Fig.8 shows that the experimental and numerical visualizations are generally in good agreement. Small deviations in the isotherms, which are most pronounced close to the top and bottom walls, are believed to be due to the final heat conduction within the walls, as well as due to technical problems of the colour analysis close to the strongly reflecting light top wall.

Investigations of the onset of convection studied for a similar case [2] show particular beneficial of LC tracers for instantaneous measurements of 2-D temperature and velocity fields. A sequence of images of the flow gives us a direct view of how, after applying a temperature jump at the hot wall, primary vertical isotherms continuously transform their shape into the final characteristic S-form (Fig.9), generating convective flow in the whole cavity.

The comparison study performed with 2-D and 3-D numerical simulation of the transient temperature and velocity fields shows that there are no serious problems with the simulation of the flow in the centre plane of the cavity. Fig. 10 shows calculated and measured velocity profiles for the centre line ( $y=0.5$ ) on the symmetry plane ( $z=0.5$ ).

The good agreement observed between the calculated flow using adiabatic TBCs and the measured two-dimensional visualizations at the centre plane breaks down when approaching the front or back walls (the nominally adiabatic vertical walls) of the cavity. It was found [15] that both the experimental isotherms and the flow structure differ from those simulated. Due to the non-adiabatic conditions on the walls, the temperature field at those walls is characterised by larger horizontal gradients. The centre of the roll becomes shifted towards one of the isothermal walls (comp. Fig.3). The straight inner spiral for the one roll system with an adiabatic TBC (Fig.7a), has in reality its ends curved towards the hot wall. For the two roll system only one spiral initially appears at the front and back wall. It splits midway between the centre and side walls into two spirals forming characteristic ‘‘cats eyes’’ in the symmetry plane. The direction of the observed inner spiral is in both cases towards centre symmetry plane. Several numerical investigations have been performed to explore

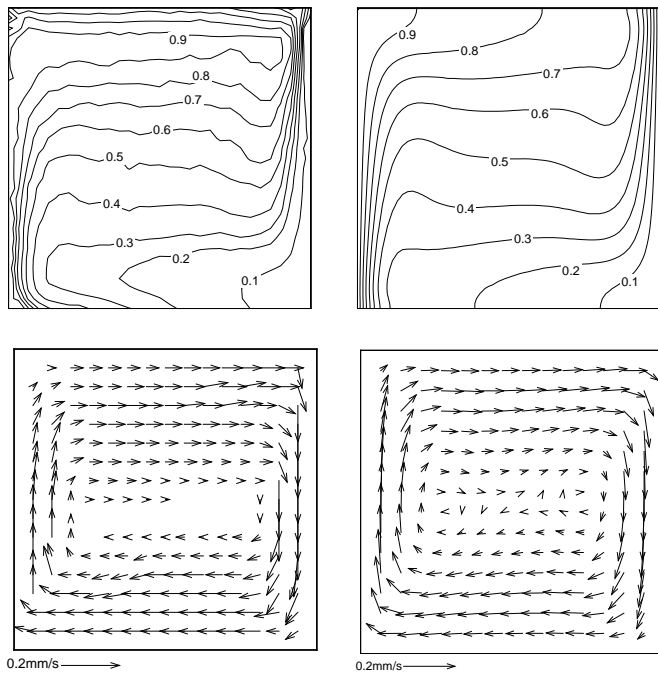


Figure 8: Measured (left) and calculated (right) non-dimensional temperature and velocity at the vertical centre plane  $z=0.5$ .

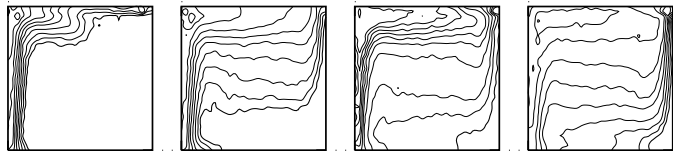


Figure 9: Transient development of isotherms measured at the centre-plane of the cavity: time  $t=2\text{min}$ ,  $10\text{min}$ ,  $20\text{min}$  and  $60\text{min}$  after the temperature  $T_h$  is applied; Initial fluid temperature  $T_o = T_c$ .  $Ra = 1.8 \cdot 10^5$ ,  $Pr = 980$ .

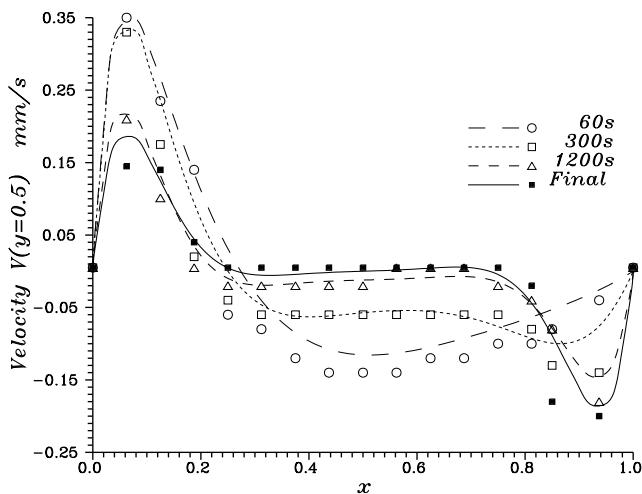


Figure 10: Transient development of the vertical velocity component along  $y=0.5$  of the symmetry plane for the cubical cavity. Time is measured from the start of heating of the plane  $x=0$ . Initial fluid temperature  $T_o = T_c$ .  $Ra = 1.66 \cdot 10^5$ ,  $Pr = 1109$ . Line - calculation, points - experiment.

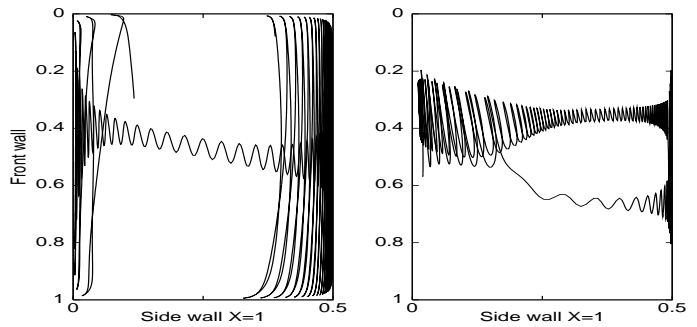


Figure 11: Top view of the streamlines calculated assuming non-adiabatic TBC.  $Pr = 6300$ , left:  $Ra = 2 \cdot 10^4$ ; right:  $Ra = 7.9 \cdot 10^4$ ; inner spirals run in both cases towards centre.

this effect. It seems that the  $z$ -component of the flow velocity responsible for the three-dimensional behaviour of tracks is extremely sensitive to TBC on all non-isothermal walls. Depending on the modelled value and direction of the heat flux, the location of the core of the spirals at the side walls may be shifted towards the hot or cold side. In this way their pitch and even direction may be easily changed (Fig.11).

Due to this sensitivity the estimation of the proper TBC for the given experiment becomes a non-trivial task, especially for the two-roll system. The trial and error method first used to fit the TBC was replaced by a process of defining an explicitly measured temperature distribution for all four non-isothermal walls. Figure 12 shows a comparison between observed particle tracks and streamlines calculated with the experimentally defined wall temperatures. Both the direction of the calculated spirals and their pitch correlate well with the measured particle tracks. The improvement obtained gives an indication of the necessity of modifications to the modeling of heat transport through and along non-isothermal walls.

A similar empirical modification of the TBCs for the higher Rayleigh number gives only a qualitative improvement. It is possible to “redirect” spirals, but modeling of the topological structures observed due to the splitting of the spiral is not possible. It is mainly due to the higher complexity of the two-roll flow.

On the other hand, in the experiment the Rayleigh number is changed simply by increasing the temperature difference  $\Delta T$ . This in turn increases the effect of the variable liquid properties. For glycerin as a fluid medium, the effect of temperature dependent viscosity produces up to 50% asymmetry in the velocity profiles. Numerical simulation shows however, that this effect is of second order as compared with the TBC, if the behaviour of three-dimensional streamlines is of interest.

The experimental investigation of the particle tracks usually helps us to answer the question, if an observed flow is the same as one obtained from the numerical simulation. However, often a new problem appears. A physical particle has a finite size, mass and buoyancy. In the creeping flow regime only particle buoyancy seems to be of importance. A good matching of particle - liquid density is not an easy task, and some remaining differences cannot be avoided due to differences in thermal expansion. Hence, small effects which appear due to these differences may become important if the long term behaviour of the tracers is stu-

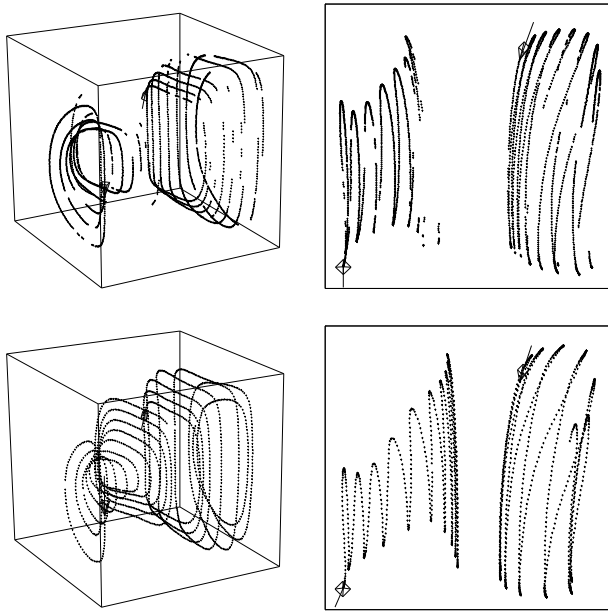


Figure 12: Particle tracks: (top) - measured, (below) - calculated using TBC from the experiment;  $Ra = 4 \cdot 10^4$ ,  $Pr = 1180$ . Isometric view of front half of the cavity (left); top view (right).

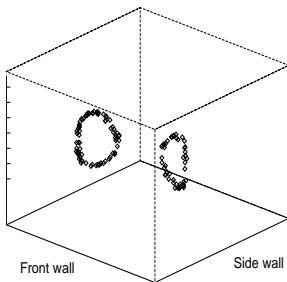


Figure 13: Calculated distribution of 300 particles, initially randomly distributed, after 140 hours.  $Ra = 10^5$ ,  $Pr = 1100$ . Particles with density 5% higher than liquid form the left ring, with 5% lower density, the right one. Both rings located about half way between front and centre plane (front half of the cavity displayed only).

died (over a time scale of several days). In a numerical study [16] it was found that due to the combined interaction of the recirculating convective flow field with the settling velocity, the particles may be trapped in some flow regions, whereas the rest of the cavity becomes particle free (Fig.13).

At the moment numerical predictions have been only partly confirmed by the experimental observations. After about 100 hours (Fig.14) we can identify an inner particle ring structure similar to the predicted one. However, also a second external particle ring appears. It seems that additional to buoyancy and Saffman forces, particle-wall interaction should also be added to the numerical model. This interaction is probably responsible for the fact that observed particles “survive” on the external ring, whereas in the numerical simulation they end up on the bottom wall. After two weeks of continuous experimental running, almost all particles which “survived” form a large (3-5mm) aggregation (Fig.15) slowly moving on the circle located close to the predicted left ring in Fig.13.

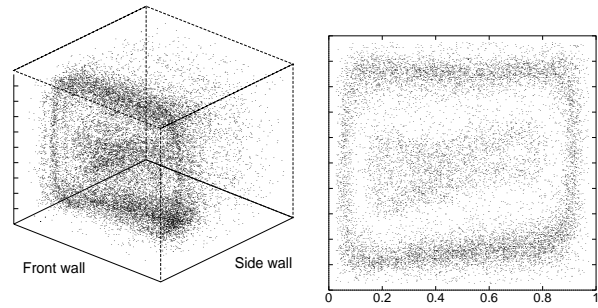


Figure 14: Distribution of particles observed after 100 hours.  $Ra = 10^5$ ,  $Pr = 1100$ . Density of particles 5% higher than liquid one; mean particle diameter 0.35mm. Isometric view of front half of the cavity (left), front view (right).

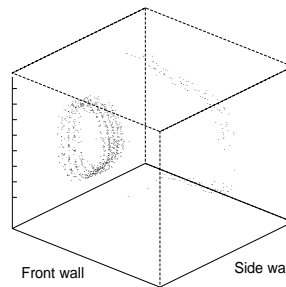


Figure 15: Distribution of “heavy” particles observed after 2 weeks; isometric view of front half of the cavity. Large agglomeration of particles is located at the left side of the cavity. There are very few other present in the box.

## 5.2. Lid cooled cavity

The onset of convection and the stability of an initially isothermal fluid in a cubical box instantaneously cooled from above have been investigated both experimentally and numerically. So far experiments have been performed with water at an initial temperature  $21^\circ C$ .

The top wall was suddenly cooled either to a temperature of  $15.5^\circ C$  or to a temperature of  $-10^\circ C$ . In the latter case, formation of ice and the effects of the density inversion of water are observed. Our interest was mainly directed towards an understanding of the transient development of the convective flow and ice front in the centre vertical plane of the cavity. The flow starts from the lid, when an initial cold thermal boundary layer becomes unstable, breaking down to four symmetrical plumes falling down along the side walls (Fig.16a). This in turn generates several recirculating zones, transporting heat and vorticity from the side walls to the centre. Within 3-5 minutes a general flow pattern is established. In the centre plane two “jets” of cold liquid are streaming along the side walls, and another one along the vertical box axis (Fig.16b). This configuration is unstable. Depending on experimental disturbances or numerical noise present, after 4-8 minutes a dramatic flow pattern transformation takes place. Passing through several strongly asymmetrical flow forms, a final configuration with a single cold “jet” along the cavity axis and a reverse flow along side walls establishes. The final state is reached after about 40 minutes. Figure 17 shows observed and calculated temperature and velocity fields in the centre symmetry plane ( $Ra = 2.7 \cdot 10^6$ ,  $T_h = 21^\circ C$ ,  $T_c = 15.5^\circ C$ ) for this configuration.

The formation of ice has been studied by decreasing the lid temperature to  $-10^\circ C$ . A complicated flow pattern appears after the convection starts which also becomes visible in the structure of the ice surface (Fig.18a). It was found that the creation of the ice layer at the lid has a stabilising

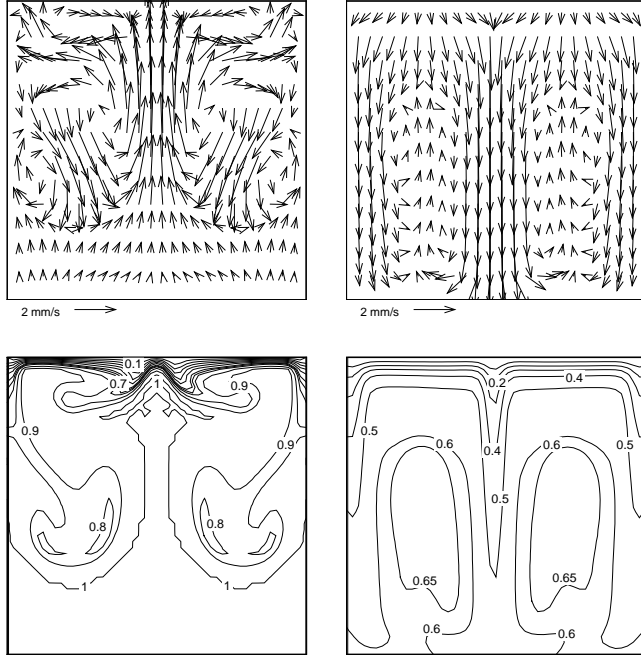


Figure 16: Onset of convection in the lid cooled cavity.  $Ra = 2.7 \cdot 10^6$ ,  $Pr = 7$ . Numerical simulation for  $t=40s$  (left) and  $t=200s$  (right). Velocity vectors and non-dimensional temperature at the centre plane  $z=0.5$ .

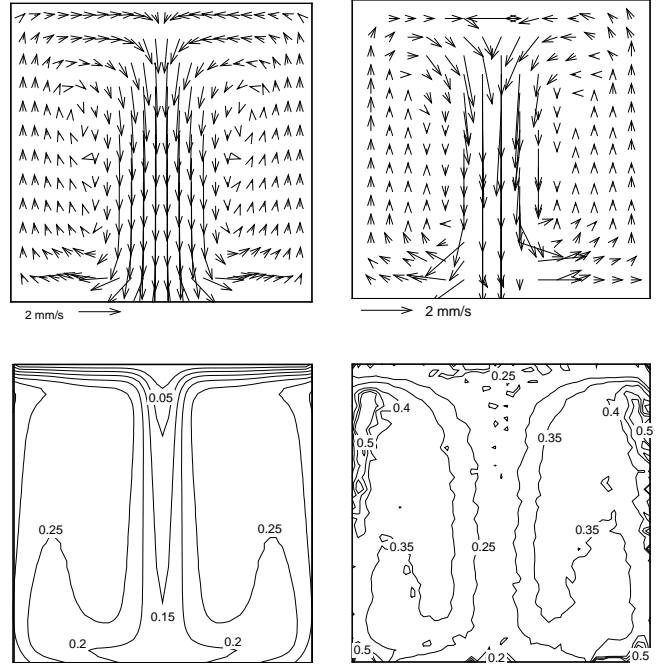


Figure 17: Convection in the lid cooled cavity at symmetry plane  $z=0.5$ . Velocity and non-dimensional temperature at the final state ( $t=60$  minutes). Numerical simulation (left); experiment (right).

effect on the flow. This is due to the symmetry of the ice solid surface, which imposes the direction and character of the flow, eliminating the instabilities observed for the pure convection case. There is also a density inversion under the lid which decelerates the main “jet” and limits a strong generation of vorticity in that region.

The overall agreement between calculated and measured characteristics of the flow (temperature distribution, velocity profiles, growth rate of ice) is relatively good. However, the measured temperature field (Fig.17) shows that numerical simulation underestimate heat flux through the side walls. Hence, the measured values of temperature are up to 30% higher as predicted. Also as in the previously discussed case, there are several differences in the fine flow details, which are difficult to control both experimentally and numerically. One seems to be the flow structure directly underneath the lid. Flow visualization shows the existence of small spiralling structures, which are generated within the thin thermal boundary layer created there. Also “large” spiralling structures responsible for the recirculating flow within each of the eight symmetrical cells across the cavity are differently oriented. Hence, the measured and calculated temperature distributions at the lid show a different symmetry (Fig.19). Our present task is to determine if this is due to wrong TBCs at the side walls, or rather to an effect due to a “weak” stability of the symmetrical flow structure, which may be easily distorted if some geometrical or thermal disturbances exist.

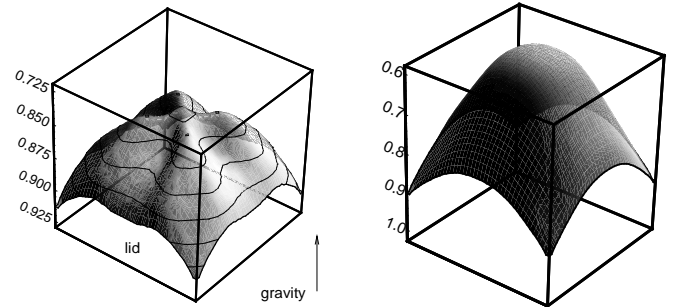


Figure 18: Ice formation at the lid cooled cavity. Ice surface calculated at 6 min (left) and 60 min (right) after cooling started (inverted view);  $Ra = 3.1 \cdot 10^6$ ,  $Pr = 13$ .

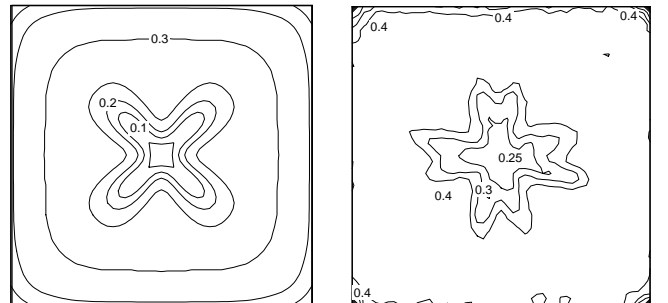


Figure 19: Calculated (left) and measured (right) non-dimensional temperature distribution underneath the cooled lid (plane  $y=0.9$ ); water,  $Ra = 2.7 \cdot 10^6$ ,  $T_h = 21^\circ C$ ,  $T_c = 15.5^\circ C$ .

## 6. CONCLUDING REMARKS

The method described for simultaneous measurement of the flow and temperature fields allows a relatively easy verification of global features of experimental and numerical simulations. Fine details of the flow can also be properly interpreted if the particle tracks are analysed. The discrepancy between the predicted and observed flow patterns can be minimized if an interactive trail and error procedure is used, modifying “weak” points in the TBCs, implementing measured temperature fields as TBCs, and improving the numerical code.

In many engineering problems such a tedious procedure may seem to be unpractical. Unfortunately, at the moment we can not offer any universal “golden” rule, which could replace it. However, it has been found that a large improvement in quality and reliability of numerical simulation can be obtained by means of validations and tuning methodologies using information obtained from the flow visualization.

## Acknowledgments

The first author wishes to thank Prof. E.-A. Müller, Prof. F. Obermeier and Prof. G.E.A. Meier for their interest and research support during his stay in MPI Göttingen.

## References

- [1] W. Hiller, T.A. Kowalewski, Simultaneous measurement of the temperature and velocity fields in thermal convective flows, in *Flow Visualization IV*, (Editor Claude Veret), pp. 617-622, Hemisphere, Paris (1987).
- [2] W.J. Hiller, St. Koch, T.A. Kowalewski, F. Stella, Onset of natural convection in a cube, *Int. J. Heat Mass Transfer*, **36**, pp.3251-3263, (1993).
- [3] St. Koch, *Berührungslose Messung von Temperatur und Geschwindigkeit in freier Konvektion*, Ph.D. dissertation in *Mitteilungen aus dem MPI Göttingen FRG*, No. 108, 1993.
- [4] H.-H. Bartels-Lehnhoff, *Erfassung dreidimensionaler Bahnlinien und Geschwindigkeitsfelder mittels automatischer Bildverarbeitung*, Ph.D. dissertation in *Mitteilungen aus dem MPI Göttingen FRG*, No. 101, 1991.
- [5] L.P. Goh, E. Leonardi, G. de Vahl Davis, *FRECON3D - Users Manual*. A program for the numerical solution of mixed convection in a three-dimensional rectangular cavity. The University of New South Wales, School of Mech. and Ind. Eng., Rep 1988/FMT/7, NSWU (1988).
- [6] G.H. Yeoh, *Natural convection in a solidifying liquid*, Ph.D. dissertation, University of New South Wales, Kensington, Australia (1993).
- [7] G. Guj, F. Stella, A vorticity-velocity method for the numerical solution of 3D Incompressible Flows, *J. Comp. Physics* **106**, pp.286-298 (1993).
- [8] G.de Vahl Davis, Natural convection of air in a square cavity: a bench mark numerical solution, *Int. J. Num. Meth. Fluids* **3**, pp.249-264, (1983).
- [9] R. Paul, *Die Erfassung von Geschwindigkeitsfeldern durch automatische Bewegungsanalyse am Beispiel einer rotierenden Flüssigkeit*, Ph.D. dissertation in *Mitteilungen aus dem MPI Göttingen FRG*, No. 102 (1991).
- [10] P. Mitgau, *Verfolgung von Teilchen in einer dreidimensionalen Konvektionsströmung*, diplom, Bericht in *MPI für Strömungsforschung* 1993.
- [11] G.D. Mallinson, G. de Vahl Davis, Three-dimensional natural convection in a box: a numerical study, *J.Fluid Mech.*, **83**, pp.1-31 (1977).
- [12] G.D. Mallinson, G. de Vahl Davis, The method of the false transient for the solution of coupled elliptic equations, *J. Comp. Physics*, **12**, pp. 435-461 (1973).
- [13] F. Stella, G. Guj, E. Leonardi, The Rayleigh-Bénard problem in intermediate bounded domains, *J. Fluid Mech.*, **254**, pp. 375-400, (1993).
- [14] W.J. Hiller, St. Koch, T.A. Kowalewski, Three-dimensional structures in laminar natural convection in a cube enclosure, *Exp. Therm. and Fluid Sci.*, **2**, pp.34-44 (1989).
- [15] W.J. Hiller, St. Koch, T.A. Kowalewski, G. de Vahl Davis, M. Behnia, Experimental and numerical investigation of natural convection in a cube with two heated side walls. *Proc. of the IUTAM Symposium Cambridge U.K.*, Aug. 13-18, 1989, (Edts. H.K. Moffat & A. Tsinober), pp. 717 - 726, CUP (1990).
- [16] A. Yarin, T.A. Kowalewski, A note on particles in three-dimensional laminar natural convection in a cube enclosure, unpublished note, 1993.